Variational Transition-state Theory and Semiclassical Tunnelling Calculations with Interpolated Corrections: A New Approach to Interfacing Electronic Structure Theory and Dynamics for Organic Reactions

Wei-Ping Hu, Yi-Ping Liu and Donald G. Truhlar
Department of Chemistry and Supercomputer Institute, University of Minnesota, Minneapolis, MN 55455-0431, USA

In variational transition-state theory (VTST) and semiclassical tunnelling calculations, especially those with semiempirical potential-energy surfaces, it is sometimes desirable to match the classical energies and vibration frequencies of some points (*e.g.* the reactant, saddle point, product, van der Waals complex, ion–molecule complex) along the minimum-energy path (MEP) and in the reaction swath with high-level results, as this can improve the accuracy. This can be accomplished by adding a correction function to the calculated energies or frequencies. In this paper, we introduce a three-point or zero-order interpolated correction method which is based on the correction at three points, in particular the saddle point and two stationary points, one on each side of the MEP. We use the corrections at these points to build a correction function for the classical energy and for each vibrational mode frequency along the MEP. The function is calibrated such that the corrected result matches the accurate values at these stationary points. The functional forms to be used depend on the shape of the MEP under consideration and the relative correction values at those points. Similar treatments are applied to the determinant of the moment of inertia tensor along the reaction path and to the potential-energy function in non-adiabatic regions of corner-cutting tunnelling paths. Once parameters in the functional forms are determined, we then use the corrected energy, frequency and moments of inertia information together with other MEP and reaction swath data, as obtained directly from the potential-energy surface, to perform new VTST calculations. Details of the implementation are presented, and applications to reaction rate calculations of the OH + $CH_4 \rightarrow H_2O + CH_3$ and $CF_3 + CD_3H \rightarrow CF_3H + CD_3$ reactions are included.

1. Introduction

The progress of electronic structure theory in providing accurate force fields for organic reagents and transition states has been dramatic in recent years. Both *ab initio*[1] and semiempirical[2] methods have contributed to a greater ability to model potential-energy surfaces[3] for chemical reactions.

In general, one wishes to focus on the reaction path,[4–11] or a somewhat wider region[12–15] (called the reaction swath), in order to concentrate one's effort on the most relevant region of the potential-energy surface. Variational transition-state theory (VTST) with multidimensional semiclassical transmission coefficients (*i.e.* VTST with semiclassical tunnelling: VTST/ST) has been developed as a practical tool for the calculation of reaction rates and kinetic isotope effects (KIEs) in terms of potential-energy surface information along the reaction path or in the reaction swath.[10c,12–31]

Several approaches are possible for interfacing electronic structure theory with VTST/ST. The most straightforward is to fit the electronic structure information to a global potential-energy function,[3] but this involves wasteful effort since it does not take account of the economy of limiting the structure calculations to the reaction path or swath. An alternative is the direct dynamics method in which electronic structure calculations are carried out and used 'directly' without a fit.[14,15,30,32–38] Recent research in our group has focused on how to do this economically while simultaneously achieving affordable accuracy. Nevertheless, for organic systems, one is typically limited in the level of electronic structure theory that may be employed by the large number of calculations required. For example, several of the direct dynamics calculations that have been carried out are based on semiempirical molecular orbital theory. The most commonly used semiempirical models are MNDO,[39] AMI[40] and PM3,[41] which are general parametrized methods defined in

the framework of the neglect of diatomic differential overlap[42] (NDDO) approximation. NDDO molecular orbital theory with specific reaction parameters[15,30,37,38] (NDDO-SRP) has been used to obtain a better representation of the potential-energy surface for individual reactions. SRP parameters can be fitted either to experiment or to selected *ab initio* data. Several VTST/ST calculations based on NDDO and NDDO-SRP methods have been carried out,[15,30,32,37,38] and these methods have proved to be very useful theoretical tools for qualitative or semiquantitative dynamics analysis.

A compromise between the global fitting and direct dynamics approaches is provided by interpolated variational transition-state theory[43–45] (IVTST). In that method, high-level *ab initio* calculations are carried out at a few points (including the reactants, saddle point and products) along the reaction path, and then all the reaction path information needed in the reaction rate calculations is interpolated based on the data at those points. This provides a practical method to include important dynamical effects in rate calculations with a minimal number of electronic structure calculations, thereby allowing as high as possible a level of theory to be used. Recently, this method has been applied to the OH + $CH_4 \rightarrow H_2O + CH_3$ reaction[44] and isotopic analogues[45] with data from correlated electronic structure calculations[46] based on a correlation-consistent polarized triple-zeta basis set,[47] and the calculated results are in good agreement with experiment.[48–50]

Both IVTST and semiempirical methods such as NDDO-SRP, despite their general applicability and anticipated wide utility, suffer from some disadvantages. In the IVTST methods, the major concern is whether the information obtained from *ab initio* calculations at the selected points is sufficient to make an accurate interpolation along the entire range of reaction path needed for the VTST/ST calculations.

Furthermore, IVTST has not been extended yet to large-curvature tunnelling cases[12,15,24–29,31,51–54] where the important swath involves more than just reaction-path information. In the semiempirical methods, one can perform many electronic structure calculations along the reaction path or swath very economically, but the major concern is whether the potential-energy surfaces are accurate enough for the dynamic calculations. One can usually fix the overall exoergicity and barrier height by using the SRP method, but it is much harder (perhaps, impossible) to fit the geometry and vibrational frequencies simultaneously. Good vibrational frequencies are usually needed for accurate reaction rate calculations, and they are crucial in the interpretation of the KIEs. Although fitting the frequencies by using the SRP method is possible in principle, no systematic prescription exists.

In this paper, we present a new interpolation method for interfacing electronic structure theory with VTST/ST calculations. In this method, the goal is to use both accurate results (usually from high-level *ab initio* calculations, but it would also be possible to take at least some of these results, *e.g.* reactant frequencies or an approximate barrier height, from experiment) at selected points along the reaction path and also semiempirical molecular orbital calculations for a much greater number of points. (The method is straightforwardly generalized to use any higher-order, more expensive level of calculations at a smaller number of points, and any less expensive method, *e.g.* a lower-level *ab initio* calculation, at a larger number of points.) Instead of interpolating the reaction-path information directly, we propose to interpolate the differences between the accurate values and the values calculated from the semiempirical surface. In other words, we are interpolating the corrections to the semiempirical values along the reaction path based on the corrections at the selected points where high-level *ab initio* calculations have been carried out. The method is also extended to treat wider reaction swaths. We think that if the semiempirical potential-energy surface is qualitatively correct, this method should provide better reaction path or swath information than the IVTST or uncorrected NDDO-SRP methods do. The interpolation method discussed below is based on corrections at three points on the reaction path, in particular the saddle point, and two stationary points, one on the reactant side of the reaction path, and the other one on the product side. The new method is called VTST-IC, VTST/ST-IC, or just IC which denotes interpolated corrections.

Collins and Ischtwan[55] have also provided a method of interpolating corrections from calculations at a higher level. Their goal, however, is different from ours. They assume that the higher-order data available comprise a set of single-point energy calculations at a subset of points on a lower-order reaction path. Thus they do not allow for higher-order hessians computed at a stationary-point geometry calculated by optimization at the higher-order level, which is our goal here.

This paper is organized as follows. Section 2 gives a brief review of the variational transition-state theory and semiclassical tunnelling approximations and an introduction to the theoretical basis of the proposed interpolation scheme. Section 3 presents the schemes proposed for interpolating reaction path or swath information along the various types of MEP. Discussion of the special procedures for low-frequency generalized normal modes is presented in Section 4. Section 5 presents results and discussion.

2. Dynamics Methods

We provide here a brief overview of the dynamics methods. In VTST/ST, the dynamics of reactive events that proceed by passing over the barrier classically are accounted for by making the fundamental no-recrossing assumption of

transition-state theory at a variationally optimized hypersurface dividing reactants from products.[18] In the present paper we use canonical variational theory in which the location of the hypersurface is optimized for a canonical ensemble from among a one-parameter sequence of generalized transition states orthogonal to the MEP in mass-scaled coordinates.[18–20] The reaction path for our VTST/ST calculations is defined as the path of steepest descents through mass-scaled (isoinertial) coordinates x from the saddle point towards reactants and products.[4,6–10,16–22] The mass-scaled coordinates for an N-atom system with masses m_i are defined in terms of atomic cartesians and the cartesians of the centre of mass by[20]

$$x_{i\gamma} = (m_i/\mu)^{1/2}(R_{i\gamma} - R_{cm,\gamma});$$

$$i = 1, 2, \ldots, N; \quad \gamma = x, y, z \qquad (1)$$

where μ is an arbitrary mass (called the scaling mass). The distance along the MEP is called s, with $s = 0$ at the saddle point, and $s < 0$ ($s > 0$) on the reactants' (products') side. We note that the MEP and the distance s are independent of the precise definition of the mass-scaled coordinates, provided they remain isoinertial,[16] *i.e.* provided they diagonalize the kinetic energy with the same mass μ for each square term.

For a canonical ensemble, the generalized transition-state rate constant of a bimolecular reaction for a generalized transition state at s at temperature T is given by

$$k^{GT}(T, s) = \sigma \frac{k_B T}{h} \frac{Q^{GT}(T, s)}{\Phi^R(T)} \exp[-V_{MEP}(s)/k_B T] \qquad (2)$$

where σ is the symmetry factor (omitted from the overall rotational partition functions) which accounts for the reaction path multiplicity, k_B is Boltzmann's constant, h is Planck's constant, $V_{MEP}(s)$ is the Born–Oppenheimer potential at s, $Q^{GT}(T, s)$ is the internal partition function at s with $V_{MEP}(s)$ as the local zero of energy, and $\Phi^R(T)$ is the reactant partition function per unit volume with respect to the overall zero of energy as the equilibrium Born–Oppenheimer potential energy of reactants infinitely apart. For a unimolecular reaction, $\Phi^R(T)$ is replaced by $Q^R(T)$, the reactant partition function. The variationally optimized reaction rate constant for a canonical ensemble is the product of the minimized value of $k^{GT}(T, s)$ obtained by varying the location of the generalized transition state and a transmission coefficient, κ, which accounts for the effects of tunnelling and non-classical reflection.

Assuming the electronic, rotational, and vibrational degrees of freedom are separable, and making the harmonic approximation for vibrations, the critical quantities needed along the reaction path for calculating $k^{GT}(T, s)$ are:[22,29,31] $V_{MEP}(s)$, the potential energy; $\omega_m(s)$, the generalized normal-mode vibrational frequencies, where subscript m designates the generalized normal mode and $m = 1, 2, \ldots, F - 1$, where F is the number of internal degrees of freedom ($3N - 5$ or $3N - 6$); and $I(s)$, the determinant of the moment of inertia tensor. In addition, for small-curvature tunnelling calculations, we will need $\mu^{SC}(s)$, the small-curvature effective mass. Furthermore, for large-curvature tunnelling calculations we need the potential energy $V(x)$ at arbitrary points in the swath that may be located more than a radius of curvature from the MEP, and hence which cannot be obtained uniquely in terms of reaction path coordinates.

We will provide more detail on the semiclassical tunnelling methods since they have evolved recently.[15,29–32] When semiclassical methods are employed, evaluation of κ involves, in general, calculating the imaginary action integral, θ, along a given tunnelling path C,

$$\theta = \int_C \sqrt{\{2\mu_{eff}(\xi)[V_{eff}(\xi) - E]\}} \, d\xi \qquad (3)$$

where μ_{eff} is the effective reduced mass for tunnelling, V_{eff} is the effective tunnelling barrier, E is the total energy, and ξ is the arc length variable of curve C. Thus corrections to $\mu_{eff}(\xi)$, $V_{eff}(\xi)$, and even the tunnelling path must be incorporated in a consistent fashion if modification has been made to the force field along the MEP. To the zeroth order, one may only have to consider corrections to the effective tunnelling barrier. However, correcting the force field also implies modification to the geometry of the potential-energy surface, and therefore, the reaction-path curvature, which affects the extent of corner cutting. In other words, consistent treatment of tunnelling in the interpolation approach depends on how we correct the geometry of the low-level potential energy surface (PES) that provides the starting point for the interpolation scheme. The geometry of the PES within the reaction swath can be represented by the stiffness of the potential [i.e. $V_{MEP}(s)$ and the $\omega_m(s)$ in the harmonic approximation] in a locally defined curvilinear coordinate system defined by F unit vectors. The unit vectors are the normalized negative gradient vector $[v(s)]^{22}$ and the generalized normal-mode vibrational unit eigenvectors $[L_m(s)]$.[9,22] These quantities, $V_{MEP}(s)$, $\omega_m(s)$, $v(s)$ and $L_m(s)$, provide all the information needed to define the set of tunnelling paths or implicit tunnelling paths, the effective reduced mass for tunnelling, and the effective tunnelling barrier in all three tunnelling approximations considered below. For this reason the difficulty of making an accurate dynamics prediction by correcting a low-level PES is reduced when this PES not only has reasonably accurate stiffness variables but also has reasonably accurate values of $v(s)$ and $L_m(s)$. The essence of our interpolation scheme is to correct $V_{MEP}(s)$ and $\omega_m(s)$ but not to correct the F unit vectors; thus the requirement that the latter are reasonable becomes particularly important. Our final semiclassical tunnelling approximations, to be discussed next, will be based on calculations for two limiting cases, namely small and large curvature of the reaction path. In the former case, tunnelling paths are defined implicitly by $\mu^{SC}(s)$, which depends only on the components of $dv(s)/ds$ along the $L_m(s)$ directions and on the $\omega_m(s)$, whereas in the latter case the tunnelling paths are constructed explicitly and they require a knowledge of the $L_m(s)$ as well.

Tunnelling is calculated from semiclassical (i.e. WKB) ground-state transmission coefficients.[15,29-32] A ground-state transmission coefficient is the thermally averaged transmission probability for a ground-state system passing the transition-state region in the exothermic direction of reaction divided by the thermally averaged transmission probability for such a system if the reaction-coordinate motion is classical, but the $F - 1$ transverse degrees of freedom are maintained in the quantized ground state. In particular, we employ the microcanonical optimized multidimensional (μOMT) tunnelling approximation to calculate the ground-state transmission coefficient, and we present here a brief review of the quantities involved.

When the reaction-path curvature can be neglected, the effective reduced mass for tunnelling is the scaling mass, and the proper tunnelling path is the MEP. Approximating the tunnelling path in this way is called the zero-curvature tunnelling (ZCT) approximation. In this case, the only quantity in the above equation that needs to be corrected is the effective tunnelling potential barrier, which is the adiabatic ground-state potential along the reaction path, called $V_a^G(s)$ and given by the sum of $V_{MEP}(s)$ and the zero-point energies corresponding to the $\omega_m(s)$.

To take the reaction-path curvature into account, we use the microcanonical optimized multidimensional tunnelling approximation,[15] which is a crude analogue of the least-action principle.[21] In this approximation, the transmission

probability is the maximum of the values calculated with two different methods, the centrifugal-dominant semiclassical adiabatic ground-state (CD-SCSAG) approximation.[29,32] which is the most accurate method for cases with a small reaction-path curvature, and the large-curvature ground-state method, version $3^{27,29}$ (LCG3), which is needed when adiabatic tunnelling through the ground-state potential is no longer the dominant mechanism.

The tunnelling path in the CD-SCSAG method is implicit, but it may be visualized as approximately corresponding to the concave-side vibrational turning points along the reaction path, and hence the effective tunnelling potential is the adiabatic ground-state potential along the reaction path. In practice, the CD-SCSAG action integral is obtained by integrating eqn. (3) along the MEP with an effective tunnelling barrier given by $V_a^G(s)$, and the effective reduced mass given by $\mu^{SC}(s)$, which depends on the frequencies $\omega_m(s)$, the components of $dv(s)/ds$ along the $L_m(s)$ directions, and the generalized normal-mode vibrational turning points $t_m(s)$, which can be calculated from the frequencies in the harmonic approximation.[29] In the harmonic approximation, an accurate $V_a^G(s)$ may be approximated using the corrected $V_{MEP}(s)$ and $\omega_m(s)$, and the correction to the force field is incorporated in the calculation of the effective reduced mass using the corrected $\omega_m(s)$. In both the ZCT and CD-SCSAG methods, the system is assumed to remain in the vibrationally adiabatic ground state throughout the tunnelling region, although outside this region the vibrations and rotations may be non-adiabatic.[56,57]

In the LCG3 method, we do not assume a single optimal tunnelling path for a given total energy. Rather, tunnelling amplitudes are evaluated along all possible straight-line paths with equal kinetic energy before and after tunnelling, and these tunnelling amplitudes are then weighted by the local speed and the vibrational period to give the transmission probability. In the LCG3 method one always calculates the semiclassical transmission probability in the exoergic direction of reaction. The effective tunnelling potential at each point along straight-line paths is taken to be the vibrationally adiabatic potential within the adiabatic regions on the reactant and product sides or it is calculated from the Born–Oppenheimer potential if the point is between these adiabatic regions. The definitions of the adiabatic and non-adiabatic regions, and the evaluation of the effective tunnelling potential barrier are discussed in detail in ref. 29. In the LCG3 approximation the tunnelling probabilities include contributions in which the system is vibrationally excited on the product side, and this is discussed in ref. 29 and 31. To be consistent with the correction along the MEP, the corrected effective tunnelling potential is calculated from the corrected $V_{MEP}(s)$ and $\omega_m(s)$ for points within the adiabatic regions. For points not in the adiabatic regions, we add a quantized vibration (QV) contribution to the Born–Oppenheimer potential, as explained below eqn. (18).

3. Types of MEP and the Corresponding Correction Functions

In the following discussion, we assume that the reaction under consideration has a saddle point, and we consider only gas-phase reactions. We will consider four types of arrangements of the relevant stationary points along the MEP. Type 1 is an MEP for a reaction with two reactant species and two product species and without intermediate complexes. Type 2 is the MEP for a reaction with two reactant species and one product species or the MEP with a well on the product side. Type 3 is the MEP for a reaction with one reactant species and two product species or the MEP with a well on the reac-

tant side. Type 4 is the MEP for a reaction with one reactant and one product or the MEP with wells on both reactant side and product side. To make the cases clearer, consider some examples. The reaction $OH + CH_4 \rightarrow H_2O + CH_3$ is type 1 if, as is usually the case for neutral reactions, we ignore the van der Waals wells in the entrance and exit valleys. However, $Cl^- + CH_3Br \rightarrow CH_3Cl + Br^-$ should be treated as type 4, i.e. we should interpolate between wells, not using asymptotic information for interpolation, since the ion–dipole complexes between the asymptotes and the saddle point are too deep to be ignored, and it would be not be reasonable to assume low-order interpolation would be valid all the way from the saddle point to the asymptotes. Another type 4 example would be the isomerization of methyl isocyanide to methyl cyanide. An example of type 3 would be $C_2H_5Cl \rightarrow C_2H_4 + HCl$, and the reverse would be type 2.

We assume that we have a low-level potential-energy surface from, e.g., semiempirical calculations, which is not accurate enough, and we need a correction function to make it more accurate. We assume we have more accurate *ab initio* calculations for the reactant, the saddle point, and two additional stationary points to be used for interpolation, depending on the type. For types 1 and 2 and unimolecular reactions of types 3 and 4, one of the three stationary points used for interpolation is also the reactant so the total number of higher-level calculations required is three. For a bimolecular type-3 or type-4 MEP, the reactant information is not used for interpolation, and one requires four high-level calculations.

In all cases the high-level calculations are used directly to compute reactant partition functions, and the new IC methods are used to correct $V_{MEP}(s)$, $\omega_m(s)$, $I(s)$, $V(x)$ and $\mu^{SC}(s)$ for generalized transition states and tunnelling calculations.

3.1 MEP Type 1

First we consider the reaction

$$A + B \rightarrow C + D \tag{I}$$

The correction function for V_{MEP} is

$$\Delta V(s) = V_{MEP, HL}(s) - V_{MEP, LL}(s) \tag{4}$$

where $V_{MEP, HL}(s)$ is the accurate (high-level) curve we seek, and LL denotes the low-level value. We know $V_{MEP, HL}(s)$ and hence $\Delta V(s)$ at $s = \pm \infty, 0$. The values of V and ΔV at $s = 0$ are called $V^{\ddagger}$ and $\Delta V^{\ddagger}$. When $\Delta V(s = 0) > \Delta V(s = \pm \infty)$ or $\Delta V(s = 0) < \Delta V(s = \pm \infty)$, we assume that the maximum or minimum of the correction function appears at $s = 0$, and we approximate it as an Eckart function, which yields

$$\Delta V(s) = \frac{AY}{1 + Y} + \frac{BY}{(1 + Y)^2} + C \tag{5a}$$

$$Y = \exp\left(\frac{s - S_0}{L}\right) \tag{5b}$$

where

$$A = \Delta V(s = +\infty) - \Delta V(s = -\infty) \tag{6a}$$

$$C = \Delta V(s = -\infty) \tag{6b}$$

$$B = (2\Delta V^{\ddagger} - A - 2C)$$
$$\pm 2[(\Delta V^{\ddagger} - C)(\Delta V^{\ddagger} - A - C)]^{1/2} \tag{6c}$$

$$S_0 = -L \ln\left(\frac{A + B}{B - A}\right) \tag{6d}$$

In eqn. (6c) the sign is positive if $\Delta V(s = 0) > \Delta V(s = \pm \infty)$ and is negative if $\Delta V(s = 0) < \Delta V(s = \pm \infty)$. At this point the range parameter L is still undetermined, so we approximate it as follows. First we fit the low-level V_{MEP} to an Eckart function at the three stationary points and at one additional point $s = s_L$ where

$$V_{LL}^{\ddagger} - V_{MEP, LL}(s = s_L) = \frac{1}{2}\{V_{LL}^{\ddagger} - V_{MEP, LL}[s = (\text{sign } s_L)\infty]\} \tag{7}$$

The sign of s_L is positive if A is positive, and it is negative if A is negative. We then discard the fitting and keep only the range parameter L. From now on, throughout this section, all equations containing L use the value determined this way.

If the correction at the saddle point is intermediate in signed value between the correction at reactant and the correction at product then we approximate the correction function with a similar Eckart function and an inverted Eckart function. First, we defined

$$D = \Delta V(s = 0) - \Delta V(s = \infty) \tag{8}$$

For $s \leqslant 0$, we approximate the correction function as an Eckart function of eqn. (4). The constants A, B, C and S_0 are determined by eqn. (6a)–(6d) with the term $\Delta V(s = \infty)$ replaced by $\Delta V(s = \infty) + 2D$.

For $s > 0$, we invert the Eckart function we used for $s \leqslant 0$, and add to it a constant term $2\Delta V^{\ddagger}$, i.e.

$$\Delta V(s) = 2\Delta V^{\ddagger} - \left(\frac{AY}{1 + Y} + \frac{BY}{(1 + Y)^2} + C\right) \tag{9}$$

A similar formulation applies to the frequency correction functions if $\Delta\omega_m(s = 0) > \Delta\omega_m(s = \pm\infty)$ or $\Delta\omega_m(s = 0) < \Delta\omega_m(s = \pm\infty)$, when

$$\Delta\omega_m(s) = \omega_{m, HL}(s) - \omega_{m, LL}(s) \tag{10}$$

In particular we define

$$\Delta\omega_m(s) = \frac{A_m Y}{1 + Y} + \frac{B_m Y}{(1 + Y)^2} + C_m \tag{11a}$$

$$Y = \exp\left(\frac{s - S_{0, m}}{L}\right) \tag{11b}$$

where

$$A_m = \Delta\omega_m(s = +\infty) - \Delta\omega_m(s = -\infty) \tag{12a}$$

$$B_m = (2\Delta\omega_m^{\ddagger} - A_m - 2C_m)$$
$$\pm 2[(\Delta\omega_m^{\ddagger} - C_m)(\Delta\omega_m^{\ddagger} - A_m - C_m)]^{1/2} \tag{12b}$$

$$C_m = \Delta\omega_m(s = -\infty) \tag{12c}$$

$$S_{0, m} = -L \ln\left(\frac{A_m + B_m}{B_m - A_m}\right) \tag{12d}$$

$$\Delta\omega_m^{\ddagger} = \Delta\omega_m(s = 0) \tag{12e}$$

and we use the same value of L as discussed below eqn. (6d). In eqn. (12b) the sign is positive if $\Delta\omega_m(s = 0) > \Delta\omega_m(s = \pm\infty)$ and is negative if $\Delta\omega_m(s = 0) < \Delta\omega_m(s = \pm\infty)$. In all cases, the modes at various points along the reaction coordinate are correlated by simply listing them in order of decreasing frequency, with no use of symmetry. Since there are more translations and usually more rotations at $s = \pm\infty$ than at finite s, the 'left-over' generalized-transition-state modes (sometimes called transition modes) are correlated to zero frequencies at $s = \pm\infty$.

If the correction to $\omega_{m, LL}$ at the saddle point is intermediate in signed value between the correction at reactant and the correction at product, then we approximate the correc-

tion function with a hyperbolic tangent function

$$\Delta\omega_m(s) = \frac{1}{2} A_m \tanh\left(\frac{s - T_{0,m}}{L}\right) + E_m \tag{13}$$

where

$$E_m = \frac{\Delta\omega_m(s = \infty) + \Delta\omega_m(s = -\infty)}{2} \tag{14a}$$

$$T_{0,m} = -\frac{L}{2} \ln\left(\frac{1 + x_m}{1 - x_m}\right) \tag{14b}$$

$$x_m = 2\frac{\Delta\omega_m^{\ddagger} - E_m}{A_m} \tag{14c}$$

The reason we treat the case of intermediate $\Delta\omega_m^{\ddagger}$ differently to the case of intermediate $\Delta V^{\ddagger}$ is that d $\Delta V/ds$ should equal zero at the saddle point, but there is not such constraint on d $\Delta\omega/ds$.

Since the determinant of moment of inertia tensor, $I(s)$, which is the product of the principal moments of inertia, of the generalized transition state approaches infinity when s approaches positive and negative infinity, we use a different approach. We set

$$I_{HL}(s) = \alpha I_{LL}(s) \tag{15}$$

where

$$\alpha = \frac{I_{HL}(s = 0)}{I_{LL}(s = 0)} \tag{16}$$

The above interpolations provide all the information required for variational transition-state calculations, including zero-curvature and small-curvature tunnelling calculations. For large-curvature tunnelling calculations, however, we need to calculate the effective potential along a set of tunnelling paths[27] that are straight lines in the mass-scaled cartesian system x. All these paths start from a point with $s = \tilde{s}_0$ and $x = x_0$ on the reactant side of the MEP in the exoergic direction and ends at a point with $s = \tilde{s}_1(\tilde{s}_0)$ and $x = x_1$ on the product side of the exoergic direction of reaction. The set of straight-line paths will be different after applying corrections to $V_{MEP}(s)$, and the corrected normal-mode frequencies will be used to test whether a point on a straight-line path is within the adiabatic region. First we compute the harmonic expansion in the adiabatic regions[27,29]

$$V(s, \{Q_m(s)\}) = V_{MEP}(s) + \frac{1}{2}\sum_{m=1}^{F-1} \mu[\omega_m(s)]^2[Q_m(s)]^2 \tag{17}$$

where $\{Q_m(s)\}_{m=1}^{F-1}$ are the generalized normal-mode coordinates at s. This expansion is computed using $V_{MEP}(s)$ and $\omega_m(s)$ corrected as described above and by assuming that $L_m(s)$ is unchanged from the low-level calculations. (After the adiabatic ground-state potential is corrected, the tunnelling path for a given energy grid point differs from the one before the IC modifications. Therefore the quadrature point on the tunnelling path after the IC modifications is at a different point in configuration space. We calculated this point from the saved $L_m(s)$ vectors from the low-level calculation.) Some of the straight-line paths also pass through a region where the adiabatic approximation based on reaction-path coordinates breaks down. In such non-adiabatic regions, the effective potential may be written

$$V_{eff}(x) = V(x) + V_{QV}(x) \tag{18}$$

where $V_{QV}(x)$ is defined by eqn. (27) of ref. 27. One defines a progress variable ζ along each straight-line path, and one can find the corrected boundaries, $\zeta_a(\tilde{s}_0)$ and $\zeta_b(\tilde{s}_0)$, of the non-adiabatic region along the straight-line tunnelling path starting at $\tilde{s}_0$ by using eqn. (23) and (24) of ref. 27. One can also

find the corrected turning points $t_m(s)$ and uncorrected curvature coupling term $B_{mF}(s)$ from eqn. (25) and (26) of ref. 27. Now, all the information required to compute the corrected $V_{QV}(x)$ is available from the above discussion, and we are left with evaluation of $\Delta V(x)$, the corrections to $V(x)$, along a straight line from $x_a(\tilde{s}_0)$ to $x_b(\tilde{s}_0)$, where $x_a(\tilde{s}_0)$ and $x_b(\tilde{s}_0)$ are the mass-scaled cartesian coordinates at $\zeta_a(\tilde{s}_0)$ and $\zeta_b(\tilde{s}_0)$, respectively.

If $\Delta V^{\ddagger}$ is intermediate in signed value between $\Delta V(\tilde{s}_0)$ and $\Delta V(\tilde{s}_1)$ we use a linear correction function

$$\Delta V(x) = a|x - x_0| + b \tag{19}$$

where

$$a = \frac{\Delta V(s = \tilde{s}_1) - \Delta V(s = \tilde{s}_0)}{|x_1 - x_0|} \tag{20a}$$

and

$$b = \Delta V(s = \tilde{s}_0) \tag{20b}$$

If the correction to the potential energy at the saddle point is larger or smaller in signed value than both the corrections at $\tilde{s}_0$ and $\tilde{s}_1$, we use a quadratic correction function

$$\Delta V(x) = \Delta V^{\ddagger} + B|x - x_c|^2 \tag{21}$$

where

$$B = \frac{\Delta V(s = \tilde{s}_0) - \Delta V^{\ddagger}}{|x_0 - x_c|^2} \tag{22a}$$

$$x_c = x_0 + (x_1 - x_0)\frac{Q}{1 + Q} \tag{22b}$$

and

$$Q = \sqrt{\left(\frac{\Delta V(s = \tilde{s}_0) - \Delta V^{\ddagger}}{\Delta V(s = \tilde{s}_1) - \Delta V^{\ddagger}}\right)} \tag{22c}$$

3.2 MEP Type 2

We now consider the reactions

$$A + B \to AB^{\ddagger} \to C \tag{II}$$

$$A + B \to AB^{\ddagger} \to C\cdots D \to C + D \tag{III}$$
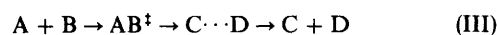
In reaction (II) there are two reactants and one product, so the product side of the MEP is finite. In reaction (III) the system first forms a complex $C\cdots D$ which is represented by a well on the product side of the MEP, before it separates into the individual final products C and D. Although the product side of the MEP is not finite in reaction (III), most VTST calculations only need the MEP information from the saddle point to the complex (and from the saddle point to reactant). So in both reactions (II) and (III) we need correction functions for the range $s = -\infty$ to $s = s_{PW}$, where s_{PW} denotes the location of the product well [in the case of reaction (II)] or the complex [in the case of reaction (III)].

For the correction function $\Delta V(s)$, if the correction at saddle point is larger or smaller in signed value than both the corrections at the reactant and at s_{PW}, then for $s \leqslant 0$, we use an Eckart function as we did in eqn. (5) and (6) but with $s = \infty$ replaced by $s = s_{PW}$. The range parameter L is determined the same way as below eqn. (6d) with s_L negative. If $s > 0$, we assume that the correction function for $V_{MEP}(s)$ has a gaussian form

$$\Delta V(s) = A_P \exp\left(-\frac{B_P}{1 - (s/s_{PW})^2}\right) + C_P \tag{23}$$

where

$$A_P = [\Delta V^{\ddagger} - \Delta V(s = s_{PW})]\exp(B_P) \tag{24a}$$

$$C_P = \Delta V(s = s_{PW}) \tag{24b}$$

and B_P still needs to be determined. (Here the subscript P denotes that it is used only for the product side. We need to change the subscript to R whenever needed in the MEP type 3 and type 4 cases, which will be discussed in the next two sections.) To determine B_P we first fit the low-level $V_{MEP}(s)$ to a cut-off gaussian function of the form of eqn. (23) at $s = 0$, $s = s_{PW}$, and an additional point on the product side at $s = s_L$. Then B_P is determined by the condition of eqn. (7) with $s = \infty$ replaced by $s = s_{PW}$. Having obtained B_P, we then discard this fit to $V_{MEP, LL}(s)$.

If the correction $\Delta V^{\ddagger}$ is intermediate in signed value between $\Delta V(s = -\infty)$ and $\Delta V(s = s_{PW})$, then for $s \leqslant 0$, we approximate the correction function for $V_{MEP}(s)$ as an Eckart function as we did in the intermediate case for an MEP type 1, but with $s = \infty$ replaced by $s = s_{PW}$ in eqn. (8) and in the discussion below it. If $0 < s \leqslant s_{PW}$, we use a cut-off gaussian function to approximate the correction function as we did in eqn. (23) and (24).

The formulation above applies equally well to the frequency correction functions with the obvious substitution of $\Delta \omega_m$ for ΔV if the correction to $\omega_{m, LL}$ at the saddle point is larger or smaller in signed value than both the corrections at reactant and at s_{PW}.

If the correction to $\omega_{m, LL}$ at the saddle point is intermediate in signed value between the correction at reactant and the correction at s_{PW}, and if $s \leqslant 0$, we approximate the frequency correction function with a hyperbolic tangent as we did in eqn. (13) and (14) but with $s = \infty$ replaced by $s = s_{PW}$. If $0 < s \leqslant s_{PW}$, we use a cut-off hyperbolic tangent to approximate the correction function

$$\Delta \omega_m(s) = \frac{1}{2} A_m \tanh\left[\frac{s - T_{0, m}}{L}\left(\frac{s_{PW}}{s_{PW} - s}\right)\right] + E_m \quad (26)$$

where A_m, E_m, L and $T_{0, m}$ all have the same values as in the hyperbolic tangent correction function for $s \leqslant 0$.

To correct $I(s)$, we use eqn. (15) and (16) even though $I(s)$ does not approach infinity at s_{PW} because one only needs the corrections in the region close to the saddle point in VTST calculations. We also use the same formulation for the corrections needed for the large-curvature tunnelling calculations as we did for the MEP type 1 case.

3.3　MEP Type 3

Next, we consider the reactions

$$A \to A^{\ddagger} \to C + D \quad (IV)$$

$$A + B \to A \cdots B \to AB^{\ddagger} \to C + D \quad (V)$$
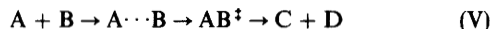
In reaction (IV) there are two products and one reactant, so the reactant side of MEP is finite. In reaction (V) the reactants first form a complex, $A \cdots B$, which is represented by a well on the reactant side of MEP, before going to reaction. In fact, reactions (IV) and (V) are just the reverse reactions of reactions (II) and (III), and all the formulae in the last section can be used with no modification by just applying the formula in the reverse direction.

3.4　MEP Type 4

Consider the reactions

$$A \to C \quad (VI)$$

$$A + B \to A \cdots B \to AB^{\ddagger} \to C \cdots D \to C + D \quad (VII)$$
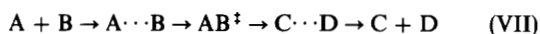
In reaction (VI) there is one reactant and one product (unimolecular reaction), so the MEP is finite on both sides. In reaction (VII) the reactants form a complex before the saddle point, and there is another well before the product, so there

are wells on both sides of MEP. We need correction functions over finite range on both sides of MEP with the left limit s_{RW} on the reactant side and the right limit s_{PW} on the product side.

For the correction function $\Delta V(s)$, we use two cut-off gaussian functions, one for the reactant side and one for the product side of the MEP regardless of the relative magnitudes of the corrections at $s = s_{RW}$, $s = 0$ and $s = s_{PW}$. Each cut-off gaussian correction function is solely determined by the corrections at $s = 0$ and either at $s = s_{RW}$ or $s = s_{PW}$ [see eqn. (23) and (24)] with B_R (for the reactant side) and B_P (for the product side) determined using the method discussed below eqn. (24b).

For the frequency correction function, if the correction at the saddle point is larger or smaller in signed value than both the corrections at $s = s_{RW}$ and $s = s_{PW}$, we use the same formulation as in the potential-energy correction functions discussed in the previous paragraph. If the correction at the saddle point is intermediate in signed value between the correction at $s = s_{RW}$ and $s = s_{PW}$, we use a cut-off hyperbolic tangent function for the entire range of MEP

$$\Delta \omega_m(s) = \frac{1}{2} A_m \tanh\left[\frac{s - T_{0, m}}{L}\left(\frac{s_{PW}}{s_{PW} - s}\right)\left(\frac{|s_{RW}|}{s - s_{RW}}\right)\right] + E_m$$
$$(27)$$

where A_m, E_m and $T_{0, m}$ are determined by eqn. (12a) and eqn. (14a)–(14c) with $s = -\infty$ replaced by $s = s_{RW}$ and $s = \infty$ replaced by $s = s_{PW}$. We use a similar method to determine L as in the MEP type 1 case as discussed below eqn. (6d) with $+\infty$ replaced by s_{PW} and $-\infty$ replaced by s_{RW} in eqn. (6a) and eqn. (7).

To correct $I(s)$, we again use eqn. (15) and (16). The corrections needed for the large-curvature tunnelling calculations are carried in the same way as for the case of MEP type 1.

4.　Special Procedures for Low-frequency Modes

4.1　IVTST-0 treatment of GTS Vibrational Frequencies

In some cases when one tries to calculate[22,29,31] the generalized normal-mode frequencies along the MEP from the saddle point towards the reactant or the product, one finds that some of the low-frequency modes of the generalized transition state, which are orthogonal to the reaction-path motion, become imaginary. This sometimes occurs because the potential-energy surface is not very accurate, or the MEP following algorithm is not fully converged, or the low-frequency modes are severely intermixed with the translational and rotational motion in the mass-scaled cartesian coordinates, but the most common cause, as discussed elsewhere,[58] is the unphysical nature of the cartesian coordinate system. When this situation cannot be avoided, we interpolate those generalized transition-state frequencies directly (as we did in the IVTST methods) based on the high-level frequencies at the saddle point and at the other two stationary points. The functional forms we used to directly interpolate the frequencies are the forms we used for the frequency correction functions, as discussed in previous sections, depending on the type of MEP and the relative magnitude of the frequencies at those three points. In particular, we use eqn. (11), (13), (23), (26) and (27). This will be called the IVTST-0 method for low-frequency modes.

4.2　Treatment of the Hindered Rotator

In the hindered rotator approximation,[29,59] besides the frequencies, we need the reduced moments of inertia to calculate the partition functions. Usually, the corrections to the

reduced moment of inertia can be made using the same formula as used for $I(s)$. However, when the situation mentioned in the previous section occurs for the modes corresponding to hindered rotators, the generalized-normal-mode eigenvectors needed[59] to calculate the uncorrected reduced moments of inertia may be unphysical; therefore, whenever we use the IVTST-0 method for the hindered rotator mode, we approximate the reduced moment of inertia of the hindered rotator along the MEP by the value at the saddle point, where the problems[58] with cartesian coordinates vanish. Since the reduced moment of inertia should not change very much in the region close to the saddle point (which is the only region where the reduced moment of inertia is typically needed), the approximation is not unreasonable.

5. Results and Discussion

5.1 OH + CH₄/CD₄

We first applied the new interpolated correction method to reaction rate calculations for the OH + CH₄ → H₂O + CH₃ and OH + CD₄ → HDO + CD₃ reactions. We present VTST/ST-IC calculations using both AM1-SRP and PM3 semiempirical potential-energy surfaces, as explained in the next paragraph. A zero-order IVTST calculation, carried out by the method of ref. 43, is also presented for comparison; the level used for zero-order IVTST is TST/ZCT, i.e. conventional transition-state theory with zero-curvature tunnelling. In addition we compare the results with the second-order IVTST calculations of ref. 44 and 45. These two sets of IVTST calculations are denoted TST/ZCT-0 and CVT/SCT-2, respectively, in Table 1. The former represents the most complete calculation one can carry out with IVTST with only three points of high-level data, the same amount as assumed here. The latter calculation requires five points of high-level data and is accordingly more expensive. The high-level data used in all these calculations, both IVTST and VTST/ST-IC, are obtained from ref. 44 and 45, where they were obtained with an adjusted correlation-consistent polarized triple-zeta

basis set[47] and Møller–Plesset second-order perturbation theory, scaling all correlation energy (SAC[60]). The semiclassical tunnelling method used for the VTST/ST-IC calculations is the μOMT method with the exit channel for the large-curvature tunnelling calculation restricted to the vibrational ground state. (We checked that tunnelling into excited states, as defined in ref. 29, makes a negligible contribution.) For both reactions there is one hindered rotation, and the four lowest-frequency modes, including the hindered rotation, were treated by the IVTST-0 method. Results from experiment[48–50] are also included for comparison.

The first step in the VTST/ST-IC calculations is to select a method for the low-level calculations. We did not use the AM1 method directly because it predicts a classical barrier height of 11.1 kcal mol⁻¹, which is ca. 4 kcal mol⁻¹ too high,[44] and an exoergicity $[V_{MEP}(s = -\infty) - V_{MEP}(s = +\infty)]$ of 21.1 kcal mol⁻¹, which is ca. 8 kcal mol⁻¹ too low. Instead, we adjusted two of the oxygen-atom semiempirical parameters,[40] U_{ss} (to a value of -119.70 eV) and U_{pp} (to a value of -79.97 eV), to fit the accurate classical barrier height (7.4 kcal mol⁻¹) and the exoergicity (13.3 kcal mol⁻¹). We call the resulting surface the AM1-SRP surface, and the VTST/ST-IC calculations based on it are called AM1-SRP-IC CVT/μOMT.

To provide a test of whether the VTST/ST-IC results are sensitive (or overly sensitive) to the choice of low-level calculations, we performed a second set of calculations using the PM3 method for the low-level implicit surface. The PM3 method predicts a classical barrier height of 10.6 kcal mol⁻¹, which is ca. 3 kcal mol⁻¹ too high and an exoergicity of 15.3 kcal mol⁻¹, which is ca. 2 kcal mol⁻¹ too low; despite these differences we decided to use the PM3 surface without changing any parameters to provide a very difficult test for the new theory.

The rates calculated by the various methods are compared with experimental values in Table 1. The table shows that the IC method significantly improves the rate contants, especially at low temperatures. We also note that the rates calculated by the uncorrected AM1-SRP method are significantly better

Table 1 Rate constants (cm³ molecule⁻¹ s⁻¹) for OH + CH₄ → H₂O + CH₃ and OH + CD₄ → H₂O + CH₃

T/K	HL TST	IVTST TST/ZCT-0	IVTST CVT/SCT-2	AM1-SRP CVT/μOMT	AM1-SRP-IC CVT/μOMT	PM3 CVT/μOMT	PM3-IC CVT/μOMT	exp.[a]
	k_H							
300	7.4 (−16)[b]	1.0 (−14)	5.7 (−15)	4.0 (−15)	5.4 (−15)	1.7 (−15)	1.3 (−14)	6.6 (−15)
350	3.0 (−15)	2.0 (−14)	1.2 (−14)	9.2 (−15)	1.1 (−14)	3.1 (−15)	2.0 (−14)	1.6 (−14)
400	8.6 (−15)	3.5 (−14)	2.3 (−14)	1.9 (−14)	2.2 (−14)	5.9 (−15)	3.4 (−14)	3.4 (−14)
600	1.2 (−13)	2.3 (−13)	1.7 (−13)	1.6 (−13)	1.6 (−13)	5.9 (−14)	2.0 (−13)	2.4 (−13)
800	5.7 (−13)	8.0 (−13)	6.4 (−13)	6.3 (−13)	6.0 (−13)	3.1 (−13)	7.1 (−13)	8.0 (−13)
1000	1.6 (−12)	2.0 (−12)	1.7 (−12)	1.6 (−12)	1.5 (−12)	1.0 (−12)	1.7 (−12)	1.9 (−12)
1500	8.8 (−12)	9.7 (−12)	8.1 (−12)	7.9 (−12)	7.3 (−12)	7.2 (−12)	7.6 (−12)	6.7 (−12)
	k_D							
300	1.1 (−16)	6.3 (−16)	6.8 (−16)	3.8 (−16)	4.6 (−16)	9.4 (−17)	1.4 (−15)	9.9 (−16)
350	5.6 (−16)	2.0 (−15)	1.9 (−15)	1.4 (−15)	1.5 (−15)	3.0 (−16)	3.4 (−15)	3.1 (−15)
400	2.0 (−15)	5.0 (−15)	4.8 (−15)	3.7 (−15)	4.2 (−15)	8.6 (−16)	7.6 (−15)	7.8 (−15)
600	4.8 (−14)	7.0 (−14)	6.1 (−14)	6.1 (−14)	6.4 (−14)	2.1 (−14)	8.4 (−14)	8.9 (−14)
800	2.9 (−13)	3.5 (−13)	3.0 (−13)	3.1 (−13)	3.3 (−13)	1.5 (−13)	3.9 (−13)	3.9 (−13)
1000	9.4 (−13)	1.1 (−12)	8.9 (−13)	9.5 (−13)	1.0 (−12)	5.9 (−13)	1.1 (−12)	n.a.[c]
1500	6.0 (−12)	6.3 (−12)	5.1 (−12)	5.4 (−12)	5.9 (−12)	5.0 (−12)	6.5 (−12)	n.a.
	k_H/k_D							
300	6.9	16.1	8.3	10.6	11.7	18.1	9.3	6.7
350	5.3	9.8	6.1	6.8	7.3	10.2	5.9	5.3
400	4.3	7.0	4.8	5.2	5.2	6.9	4.5	4.3
600	2.6	3.2	2.8	2.6	2.5	2.8	2.4	2.7
800	2.0	2.3	2.2	2.0	1.8	2.1	1.8	2.0
1000	1.7	1.9	1.9	1.7	1.5	1.7	1.5	n.a.
1500	1.5	1.5	1.6	1.5	1.2	1.4	1.2	n.a.

[a] Experimental results for CH₄ from ref. 50 for $T \leqslant 800$ K and from ref. 48 for $T > 800$ K, experimental results for CD₄ from ref. 50. [b] Power of 10 in parentheses. [c] Not available.

Table 2 Rates calculated with small- and large-curvature tunnelling methods

T/K	CVT/SCT			CVT/LCT	
	IVTST-2[a]	AM1-SRP-IC	PM3-IC	AM1-SRP-IC	PM3-IC
k_H					
300	5.7 (−15)[b]	5.4 (−15)	6.4 (−15)	2.0 (−15)	1.1 (−14)
350	1.2 (−14)	1.1 (−14)	1.4 (−14)	5.0 (−15)	1.8 (−14)
400	2.3 (−14)	2.2 (−14)	2.7 (−14)	1.1 (−14)	2.9 (−14)
600	1.7 (−13)	1.6 (−13)	1.9 (−13)	1.2 (−13)	1.8 (−13)
800	6.4 (−13)	6.0 (−13)	6.9 (−13)	5.0 (−13)	6.4 (−13)
1000	1.7 (−12)	1.5 (−12)	1.7 (−12)	1.4 (−12)	1.6 (−12)
1500	8.1 (−12)	7.3 (−12)	7.5 (−12)	7.0 (−12)	7.3 (−12)
k_D					
300	6.8 (−16)	4.6 (−16)	1.2 (−15)	2.3 (−16)	9.4 (−16)
350	1.9 (−15)	1.5 (−15)	3.2 (−15)	9.3 (−16)	2.3 (−15)
400	4.8 (−15)	4.2 (−15)	7.4 (−15)	2.9 (−15)	5.3 (−15)
600	6.1 (−14)	6.4 (−14)	8.4 (−14)	5.4 (−14)	6.9 (−14)
800	3.0 (−13)	3.3 (−13)	3.9 (−13)	3.0 (−13)	3.5 (−13)
1000	8.9 (−13)	1.0 (−12)	1.1 (−12)	9.4 (−13)	1.1 (−12)
1500	5.1 (−12)	5.9 (−12)	6.5 (−12)	5.7 (−12)	6.3 (−12)

[a] From ref. 44 and 45. [b] Power of 10 in parentheses.

than the uncorrected PM3 rates. This is not surprising because we fitted the barrier and exoergicity to the accurate values in the former case. Without this new IC method, the most complete calculation one can carry out with the high-level data available at three points is a zero-order IVTST calculation[43] with conventional transition-state theory and zero-curvature tunnelling. The IC method enables one to carry out canonical variational transition-state theory calculations with higher-level tunnelling calculations, i.e. small-curvature, large-curvature and microcanonical optimized multidimensional tunnelling calculations, and this results in better calculated rates at lower temperatures.

The bottom part of Table 1 shows the kinetic isotope effects (KIEs) calculated by the CVT/μOMT method and other methods. The IC procedure significantly improves the accuracy of the PM3 KIEs at low temperatures. At high temperatures, all methods agree well with the experiments.

Table 2 lists the calculated rates by the small-curvature and large-curvature tunnelling methods in the second-order IVTST[44] and IC calculations. In the PM3-IC calculations for CH_4, the large-curvature tunnelling mechanism is dominant at energies below 37.1 kcal mol^{-1} which is ca. 3.1 kcal mol^{-1} below the maximum of $V_a^G(s)$. For CD_4 the large-curvature tunnelling mechanism is dominant at energies below 28.9 kcal mol^{-1} which is ca. 4.3 kcal mol^{-1} below the maximum of the $V_a^G(s)$. In the AM1-SRP-IC calculations, however, the small-curvature tunnelling mechanism is dominant at all energies in both reactions so that the μOMT method becomes equivalent to the SCT method. Table 2 shows very good agreement between the two ST-IC calculations, but at low temperature the LCT-IC calculations are sensitive to the choice of underlying low-level surface.

Fig. 1 and 2 show the uncorrected and corrected adiabatic ground-state energy profiles [$V_a^G(s)$] along the reaction paths.

5.2 $CF_3 + CD_3H$

We have also applied the IC method to calculate rate constants for $CF_3 + CD_3H \rightarrow CF_3H + CD_3$ and $CF_3 + CD_3H \rightarrow CF_3D + CD_2H$. To demonstrate the usefulness of the new method, we take the previous[15] AM1-SRP calculations (with parameter set[15] 2, which leads to good agreement with experiment) as the high-level ones, and we try to reproduce them with interpolated corrections to a much cruder semiempirical molecular orbital calculation. In particular, we created a new MNDO-SRP surface to use as the
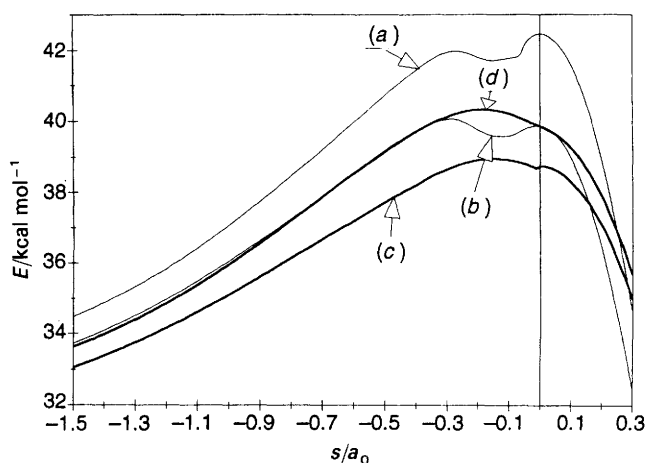

Fig. 1 Adiabatic ground-state energy curve [$V_a^G(s)$] as a function of distance along the reaction path for $OH + CH_4 \rightarrow H_2O + CH_3$ reaction. (a) PM3, (b) PM3-IC, (c) AM1-SRP, (d) AM1-SRP-IC.

low-level method. In other words, we treated the second AM1-SRP surface used in the previous work[15] as the high-level surface, and we used a much less accurate MNDO-SRP surface as the low-level surface. In MNDO-SRP surface we changed one of the fluorine parameters, U_{PP} (to a value of
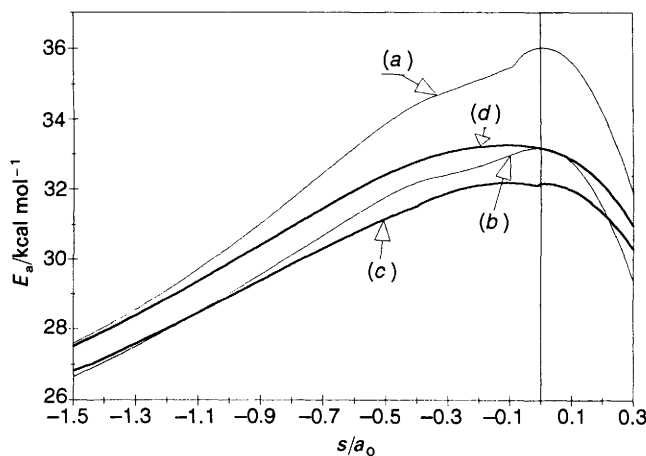

Fig. 2 Adiabatic ground-state energy curve [$V_a^G(s)$] as a function of distance along the reaction path for $OH + CD_4 \rightarrow HDO + CD_3$ reaction. (a) PM3, (b) PM3-IC, (c) AM1-SRP, (d) AM1-SRP-IC.

Table 3 Rate constants (cm^3 molecule^{-1} s^{-1}) for $CF_3 + CD_3H \rightarrow CF_3H + CD_3$ and $CF_3 + CD_3H \rightarrow CF_3D + CD_2H$

T/K	HL TST	IVTST TST/ZCT-0	HL TST/ZCT[a]	HL CVT/μOMT[a]	MNDO-SRP CVT/μOMT	MNDO-SRP-IC CVT/μOMT
	k_H					
300	8.9 (−23)[b]	1.0 (−20)	9.2 (−22)	6.0 (−21)	3.8 (−26)	2.4 (−21)
350	2.0 (−21)	5.1 (−20)	1.2 (−20)	4.0 (−20)	1.2 (−24)	2.6 (−20)
400	2.2 (−20)	2.3 (−19)	8.8 (−20)	2.0 (−19)	1.9 (−23)	1.7 (−19)
600	7.7 (−18)	1.9 (−17)	1.4 (−17)	1.8 (−17)	2.2 (−20)	2.1 (−17)
800	1.9 (−16)	3.1 (−16)	2.7 (−16)	2.6 (−16)	1.2 (−18)	3.4 (−16)
1000	1.5 (−15)	2.1 (−15)	1.9 (−15)	1.7 (−15)	1.7 (−17)	2.2 (−15)
1500	3.4 (−14)	3.9 (−14)	3.7 (−14)	3.0 (−14)	9.4 (−16)	4.1 (−14)
	k_D					
300	5.5 (−23)	1.1 (−21)	4.1 (−22)	1.2 (−21)	5.8 (−27)	6.0 (−22)
350	1.6 (−21)	1.2 (−20)	6.8 (−21)	1.2 (−20)	2.8 (−25)	9.2 (−21)
400	2.0 (−20)	8.6 (−20)	6.1 (−20)	8.3 (−20)	6.0 (−24)	7.9 (−20)
600	1.1 (−17)	1.9 (−17)	1.7 (−17)	1.6 (−17)	1.7 (−20)	2.0 (−17)
800	3.3 (−16)	4.5 (−16)	4.1 (−16)	3.6 (−16)	1.4 (−18)	4.6 (−16)
1000	3.0 (−15)	3.7 (−15)	3.3 (−15)	2.9 (−15)	2.6 (−17)	3.7 (−15)
1500	7.9 (−14)	8.6 (−14)	7.9 (−14)	6.5 (−14)	1.9 (−15)	8.6 (−14)
	k_H/k_D					
300	1.6	9.2	2.2	5.2	6.6	4.0
350	1.3	4.4	1.8	3.4	4.3	2.8
400	1.1	2.6	1.4	2.4	3.2	2.2
600	0.7	1.0	0.8	1.1	1.3	1.1
800	0.6	0.7	0.7	0.7	0.9	0.7
1000	0.5	0.6	0.6	0.6	0.7	0.6
1500	0.4	0.5	0.5	0.5	0.5	0.5

[a] From ref. 15. [b] Power of 10 in parentheses.

−108.94 eV), to make the exoergicity very close to the experimental value (0.7 kcal mol^{-1}) while the classical barrier is still 6.6 kcal mol^{-1} higher than the barrier (14.6 kcal mol^{-1}) predicted by the AM1-SRP surface. The rates were calculated on both the low-level MNDO-SRP surface and the corrected MNDO-SRP-IC surface using the CVT/μOMT method with the exit channel for the large-curvature tunnelling calculation restricted to the vibrational ground state. (Once again, we found that tunnelling into excited states makes a negligible contribution.) For both reactions, there is one hindered rotation, and the five lowest-frequency modes, including the hindered rotation, were treated by the IVTST-0 method.

Table 3 shows high-level, IVTST, low-level and corrected results for both reactions. At medium and high temperatures, the IC calculations reproduced the high-level results quite well, even with a 6.6 kcal mol^{-1} correction in the barrier. At low temperatures, the new method predicts the hydrogen-transfer rates to be about a factor of two too low. But considering the correction to the classical energy at the saddle point is ca. 6.6 kcal mol^{-1}, the results are still very encouraging. Fig. 3 and 4 show the uncorrected and corrected $V_a^G(s)$ for both reactions.

Table 4 lists the rates calculated by the small- and large-curvature tunnelling methods. We note that the IC calculations not only reproduced the high-level CVT/μOMT rates very well, but they also reproduced the previous CVT/SCT and CVT/LCT rates. Thus we obtain not only the same rates but the same picture of the reaction. In the calculations for the $CF_3 + CD_3H \rightarrow CF_3H + CD_3$ reaction, the large-curvature tunnelling mechanism is dominant at all energies. For $CF_3 + CD_3H \rightarrow CF_3D + CD_2H$ reaction, the large-curvature tunnelling mechanism is dominant below 40.3 kcal mol^{-1} which is 3.2 kcal mol^{-1} below the maximum of the $V_a^G(s)$.

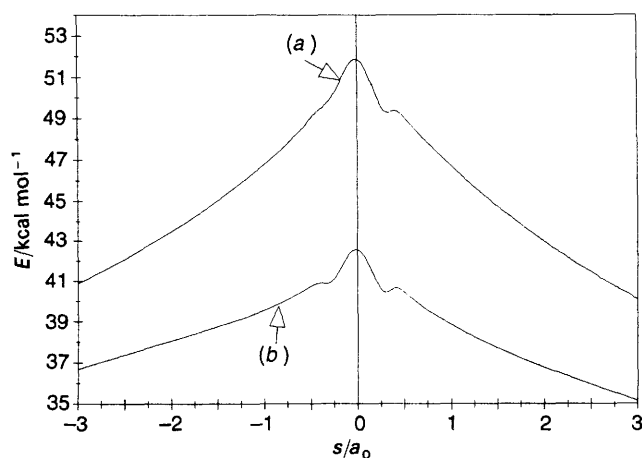**Fig. 3** Adiabatic ground-state energy curve [$V_a^G(s)$] as a function of distance along the reaction path for $CF_3 + CD_3H \rightarrow CF_3H + CD_3$ reaction. (a) MNDO-SRP, (b) MNDO-SRP-IC.

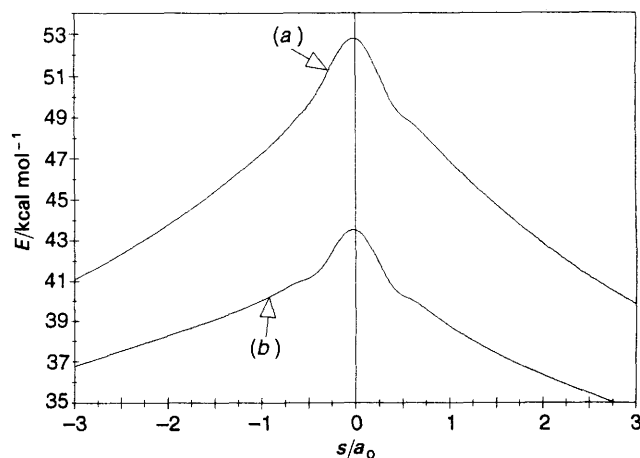**Fig. 4** Adiabatic ground-state energy curve [$V_a^G(s)$] as a function of distance along the reaction path for $CF_3 + CD_3H \rightarrow CF_3D + CD_2H$ reaction. (a) MNDO-SRP, (b) MNDO-SRP-IC.

Table 4 Rates calculated with small- and large-curvature tunnelling methods

	CVT/SCT		CVT/LCT	
T/K	high level	MNDO-SRP-IC	high level	MNDO-SRP-IC
	k_H			
300	1.8 $(-21)^a$	8.7 (-22)	5.9 (-21)	2.4 (-21)
350	1.7 (-20)	1.2 (-20)	3.9 (-20)	2.6 (-20)
400	1.1 (-19)	8.9 (-20)	2.0 (-19)	1.7 (-19)
600	1.5 (-17)	1.5 (-17)	1.7 (-17)	2.1 (-17)
800	2.4 (-16)	2.8 (-16)	2.5 (-16)	3.4 (-16)
1000	1.6 (-15)	2.0 (-15)	1.6 (-15)	2.2 (-15)
1500	3.0 (-14)	3.8 (-14)	3.0 (-14)	4.1 (-14)
	k_D			
300	7.2 (-22)	5.5 (-22)	9.6 (-22)	4.6 (-22)
350	9.2 (-21)	8.6 (-21)	9.5 (-21)	7.1 (-21)
400	7.2 (-20)	7.6 (-20)	6.6 (-20)	6.3 (-20)
600	1.6 (-17)	2.0 (-17)	1.4 (-17)	1.7 (-17)
800	3.6 (-16)	4.6 (-16)	3.4 (-16)	4.3 (-16)
1000	2.9 (-15)	3.7 (-15)	2.7 (-15)	3.5 (-15)
1500	6.5 (-14)	8.6 (-14)	6.3 (-14)	8.4 (-14)

^{a} Power of 10 in parentheses.

6. Concluding Remarks

Semiempirical electronic structure calculations provide an economical way of exploring potential-energy surfaces and carrying out dynamics calculations. However, in many situations, semiempirical methods alone cannot provide satisfactory accuracy for quantitative dynamics calculations. Some improvements are possible using SRP methods, but it is hard to make all the vibrational frequencies accurate with a single set of parameters. High-level *ab initio* calculations can provide relatively better accuracy, but they are usually too expensive to calculate enough important features of a polyatomic potential-energy surface for VTST/ST calculations. The purpose of the present interpolated correction method is to provide a way of using semiempirical potential-energy surface to do dynamics calculations while achieving good accuracy without spending too much more computational effort. In the current method, one only needs accurate data at three or four points along the reaction path, including reactants, together with semiempirical calculations at many points, to obtain the forward VTST/ST reaction rates. The interpolated correction method presented here is general enough to treat any unimolecular or bimolecular reaction with either small-curvature or large-curvature tunnelling, while the available IVTST method can only be used to treat bimolecular reactions with type-1 MEPs, and small-curvature tunnelling. We believe that the generality and flexibility of the new method will make it a very useful tool for studying a large variety of organic reactions.

7. Summary

We have proposed a new interpolated correction method for interfacing electronic structure theory and dynamics calculations. A detailed formulation has been presented. The method is validated by applications to rate calculations on $OH + CH_4 \rightarrow H_2O + CH_3$ and $CF_3 + CD_3H$. We believe that this method can be used to study many organic reactions, and we think it will make dynamics calculations with semiempirical potential-energy surface much more accurate and useful.

References

1 C. W. Bauschlicher and S. R. Langhoff, *Science*, 1991, **254**, 394.
2 J. J. P. Stewart, *Methods Comput. Chem.*, 1990, **1**, 45.
3 D. G. Truhlar, R. Steckler and M. S. Gordon, *Chem. Rev.*, 1987, **87**, 217.
4 I. Shavitt, Theoretical Chemistry Laboratory Report No. WIS-AEC-23, University of Wisconsin, Madison, 1959.
5 G. L. Hofacker, *Z. Naturforsch., Teil A*, 1963, **18**, 607.
6 R. A. Marcus, *J. Chem. Phys.*, 1966, **45**, 4493; 1968, **49**, 2610.
7 D. G. Truhlar and A. Kupperman, *J. Am. Chem. Soc.*, 1971, **93**, 1840.
8 K. Fukui, in *The World of Quantum Chemistry*, ed. R. Daudel and B. Pullwan, D. Reidel, Dordrecht, 1974, p. 113.
9 W. H. Miller, N. C. Handy and J. E. Adams, *J. Chem. Phys.*, 1980, **72**, 99.
10 (a) K. Morokuma and S. Kato, in *Potential Energy Surface and Dynamics Calculations*, ed. D. G. Truhlar, Plenum Press, New York, 1981, p. 243; (b) W. H. Miller, in ref. 10(a), p. 265; (c) B. C. Garrett, D. G. Truhlar and R. S. Grev, in ref. 10(a), p. 587.
11 M. L. McKee and M. Page, *Methods Comput. Chem.*, 1993, **4**, 35.
12 B. C. Garrett, D. G. Truhlar, A. F. Wagner and T. H. Dunning Jr., *J. Chem. Phys.*, 1983, **78**, 4400.
13 D. G. Truhlar, F. B. Brown, R. Steckler and A. D. Isaacson, in *The Theory of Chemical Reaction Dynamics*, ed. by D. C. Clary, D. Reidel, Dordrecht, 1986, p. 285.
14 D. G. Truhlar and M. S. Gordon, *Science*, 1990, **249**, 491.
15 Y-P. Liu, D-h. Lu, A. Gonzalez-Lafont, D. G. Truhlar and B. C. Garrett, *J. Am. Chem. Soc.*, 1993, **115**, 7806.
16 B. C. Garrett and D. G. Truhlar, *J. Phys. Chem.*, 1979; **83**, 1079; 1983, **87**, 4553 (E).
17 B. C. Garrett and D. G. Truhlar, *J. Am. Chem. Soc.*, 1979, **101**, 4534.
18 D. G. Truhlar and B. C. Garrett, *Acc. Chem. Res.*, 1980, **13**, 440.
19 D. G. Truhlar, A. D. Isaacson, R. T. Skodje and B. C. Garrett, *J. Phys. Chem.*, 1982, **86**, 2252.
20 A. D. Isaacson and D. G. Truhlar, *J. Chem. Phys.*, 1982, **76**, 1380.
21 B. C. Garrett and D. G. Truhlar, *J. Chem. Phys.*, 1983, **79**, 4931.
22 D. G. Truhlar, A. D. Isaacson and B. C. Garrett, in *Theory of Chemical Reaction Dynamics*, ed. M. Baer, CRC Press, Boca Raton, FL, 1985, vol. 4, p. 65.
23 D. G. Truhlar and B. C. Garrett, *Annu. Rev. Phys. Chem.*, 1984, **35**, 159.
24 B. C. Garrett, N. Abusalbi, D. J. Kouri and D. G. Truhlar, *J. Chem. Phys.*, 1985, **83**, 2252.
25 M. M. Kreevoy, D. Ostovic, D. G. Truhlar and B. C. Garrett, *J. Phys. Chem.*, 1986, **90**, 3766.
26 D. G. Truhlar and B. C. Garrett, *J. Chim. Phys.*, 1987, **84**, 365.
27 B. C. Garrett, J. Joseph, T. N. Truong and D. G. Truhlar, *Chem. Phys.*, 1989, **136**, 271; 1990, **140**, 207(E).
28 Y. Kim, D. G. Truhlar and M. M. Kreevoy, *J. Am. Chem. Soc.*, 1991, **113**, 7837.
29 D-h. Lu, T. N. Truong, V. S. Melissas, G. C. Lynch, Y-P. Liu, B. C. Garrett, R. Steckler, A. D. Isaacson, S. N. Rai, G. C. Hancock, J. G. Lauderdale, T. Joseph and D. G. Truhlar, *Comput. Phys. Commun.*, 1992, **71**, 235.
30 D. G. Truhlar, D-h. Lu, S. C. Tucker, X. G. Zhao, A. Gonzalez-Lafont, T. N. Truong, D. Maurice, Y-P. Liu and G. C. Lynch, *ACS Symp. Ser.*, 1992, **502**, 16.
31 T. N. Truong, D-h. Liu and G. C. Lynch, Y-P. Liu, V. S. Melissas, J. J. P. Stewart, R. Steckler, B. C. Garrett, A. D. Isaacson, A. Gonzalez-Lafont, S. N. Rai, G. C. Hancock, T. Joseph and D. G. Truhlar, *Comput. Phys. Commun.*, 1993, **75**, 143.
32 Y-P. Liu, G. C. Lynch, T. N. Truong, D-h. Lu, D. G. Truhlar and B. C. Garrett, *J. Am. Chem. Soc.*, 1993, **115**, 2408.
33 C. Doubleday Jr., J. W. McIver Jr. and M. Page, *J. Phys. Chem.*, 1988, **92**, 4367.
34 K. K. Baldridge, M. S. Gordon, R. Steckler and D. G. Truhlar, *J. Phys. Chem.*, 1989, **93**, 5107.
35 B. C. Garrett, M. L. Koszykowski, C. F. Melius and M. Page, *J. Phys. Chem.*, 1990, **94**, 7096.
36 B. C. Garrett, C. F. Melius and M. Page, in *Theoretical and Computational Models for Organic Chemistry*, ed. S. J. Formosinho, I. G. Csizmadia and L. G. Arnaut, Kluwer, Dordrecht, 1991, p. 35.
37 A. Gonzalez-Lafont, T. N. Truong and D. G. Truhlar, *J. Phys. Chem.*, 1991, **95**, 4618.
38 A. A. Viggiano, J. S. Pashkewitz, R. A. Morris and J. F. Paulson,

A. Gonzalez-Lafont and D. G. Truhlar, *J. Am. Chem. Soc.*, 1991, **113**, 9404.

39 M. J. S. Dewar and W. Thiel, *J. Am. Chem. Soc.*, 1977, **99**, 4899.

40 M. J. S. Dewar, E. G. Zoebisch, E. F. Healy and J. J. P. Stewart, *J. Am. Chem. Soc.*, 1985, **107**, 3902.

41 J. J. P. Stewart, *J. Comput. Chem.*, 1989, **10**, 209; 221.

42 J. A. Pople, D. P. Santry and G. A. Segal, *J. Chem. Phys.*, 1965, **43**, S129.

43 A. Gonzalez-Lafont, T. N. Truong and D. G. Truhlar, *J. Chem. Phys.*, 1991, **95**, 8875.

44 V. S. Melissas and D. G. Truhlar, *J. Chem. Phys.*, 1993, **99**, 1013.

45 V. S. Melissas and D. G. Truhlar, *J. Chem. Phys.*, 1993, **99**, 3542.

46 M. J. Frisch, G. W. Trucks, J. B. Foresman, H. B. Schlegel, K. Raghavachari, M. A. Robb, J. S. Binkley, C. Gonzalez, D. J. Defrees, D. J. Fox, R. A. Whiteside, R. Seeger, C. F. Melius, J. Baker, R. L. Martin, L. R. Kahn, J. J. P. Stewart, S. Topiol and J. A. Pople, Gaussian 90, Gaussian, Inc., Pittsburgh, PA, 1990.

47 T. H. Dunning Jr., *J. Chem. Phys.*, 1989, **90**, 1007.

48 R. Atkinson, *J. Phys. Chem. Ref. Data*, 1989, **1**, 18.

49 G. L. Vaghjiani and A. R. Ravishankara, *Nature (London)*, 1991, **350**, 406.

50 J. R. Dunlop and F. P. Tully, *J. Phys. Chem.*, 1993, **97**, 11148.

51 A. I. Shushin and M. Ya. Ovchinnikova, *Teor. Eksp. Khim.*, 1975, **11**, 445 [Engl. transl.: *Theor. Exp. Chem.*, 1975, **11**, 375].

52 Y. Ovchinnikova, *Chem. Phys.*, 1979, **36**, 85.

53 V. K. Babamov and R. A. Marcus, *J. Chem. Phys.*, 1981, **74**, 1790.

54 V. K. Babamov, V. Lopez and R. A. Marcus, *J. Chem. Phys.*, 1983, **78**, 5621.

55 M. A. Collins and J. Ischtwan, *J. Chem. Phys.*, 1990, **93**, 4938.

56 G. C. Lynch, P. Halvick, D. G. Truhlar, B. C. Garrett, D. W. Schwenke and D. J. Kouri, *Z. Naturforsch, Teil A*, 1989, **44**, 427.

57 D. C. Chatfield, R. S. Friedman, D. G. Truhlar and D. W. Schwenke, *Faraday Discuss. Chem. Soc.*, 1991, **91**, 289.

58 G. A. Natanson, B. C. Garrett, T. N. Truong, T. Joseph and D. G. Truhlar, *J. Chem. Phys.*, 1991, **94**, 7875.

59 D. G. Truhlar, *J. Comput. Chem.*, 1991, **12**, 266.

60 M. S. Gordon and D. G. Truhlar, *J. Am. Chem. Soc.*, 1986, **108**, 5412.